MICRO-PORE-SIZE ANALYSIS OF A FRIABLE LOESS

Rodney J. Huang, University of California, Berkeley; and
Turgut Demirel, Iowa State University

The sorption isotherm method was used to determine the pore-size distribution of a friable Iowa loess. Both the adsorption and the desorption branches were used for pore-size distribution analysis. The difference between the 2 branches was interpreted as an indication of the extent of constrictions within the pore structure according to McBain's "ink-bottle" theory. Pore-size distribution curves obtained from the adsorption isotherm were compatible with mercury porosimetry results. Procedures for evaluation of pore-size distribution from sorption data are described, and the pore-size range is noted.

THE TOTAL specific surface area of a porous solid, the distribution of total surface area, and the pore-volume distribution as a function of pore sizes have become progressively more important in understanding chemical and physical behavior of porous materials. Those characteristics have long been recognized as important, for example, in the assessment of the chemical activity of catalysts.

Soil structure has long been recognized as important in the field of soil mechanics. Significant advances have been made toward its determination and toward understanding its effect on the mechanistic behavior of soils (1, 2), but the first significant approach to the problem through pore-size distribution has been made rather recently by Diamond and his coworkers (3, 4).

Two independent methods exist for pore-size distribution analysis. The first, the mercury-injection method, was suggested by Washburn in 1921 (5) and was later fully developed by Ritter and Drake (6). The second, the isotherm method, was proposed by Wheeler in 1945 and was further developed by him and others (7, 8, 9, 10, 11, 12). In an extensive investigation undertaken at Iowa State University to correlate the engineering behavior of soils with soil structure (13), both of those techniques were used. The results of the mercury-injection method on disturbed and undisturbed samples of a friable Iowa loess are reported by Badger and Lohnes (14). The isotherm method was used only for the undisturbed loess sample, and the results obtained are presented, analyzed, and compared with the results of mercury-injection method in this paper.

SORPTION ISOTHERM METHOD FOR PORE-SIZE DISTRIBUTION ANALYSIS

Analysis of sorption isotherms has been extensively used to study the pore structure of various materials. Most of the methods developed during the past 25 years make use of Kelvin's capillary condensation equation and Brunauer, Emmett, and Teller's multilayer adsorption theory (15). The starting point of those methods is the equation proposed by Wheeler in 1946 (7, 8, 10). The first method to enjoy a universal acceptance was developed by Barrett, Joyner, and Halenda in 1951 (10) and is now known as the BJH method. The methods developed since then, such as those of Cranston and Inkley (12) and Pierce (11), have been revisions of the BJH method. There are other commonalities of those methods:

1. The use of nitrogen gas as the adsorbate;

Sponsored by Committee on Physicochemical Phenomena in Soils.

2. The assumption that the Kelvin radius of capillary condensation is equal to the pore radius minus the thickness of the adsorbed film; and

3. The evaluation of the adsorbed film thickness from nitrogen adsorption isotherms on nonporous adsorbents (t-curves—sorption isotherm depicted by film thickness versus relative pressure), which impose on the flexibility of the method and on the interpretation of the results the restrictions of (a) adsorbate limited to nitrogen, (b) pore shapes assumed to be cylindrical, and (c) a somewhat arbitrary film thickness (t-curves) because all data used for those methods are obtained from other so-called representative nonporous adsorbents.

Recently Brunauer and coworkers (16, 17, 18, 19, 20, 21) published a series of papers leading to the development of new methods for micro- and macro-pore-size distribution analyses. They have replaced the Kelvin radius with hydraulic radius (16) and based the adsorbed film thickness on the value of the BET parameter C (18, 21). That broadens the physical meaning of pore-size distribution analyses and eliminates most of the uncertainties from the evaluation of adsorbed film thickness.

However, for consistency with mercury porosimetry data, the pore-size distribution in the present paper is expressed in terms of Kelvin radii rather than hydraulic radii. The adsorbed film thicknesses were taken from Brunauer et al. (21) on the basis of BET parameter C. The method of analysis used is that of Pierce (11) offered in 1953. The Pierce method was selected because of its simplicity and clarity in spite of its unpopularity. An outline of the method is given below.

The vapor pressure p of a liquid adsorbate condensed in a capillary of radius r_k (Kelvin radius) and in equilibrium with its vapor is given by the following Kelvin equation if the capillary is completely wettable by the adsorbate:

$$\ln p/p_o = \frac{-2\,\gamma\,\overline{V}}{RT\,r_k} \tag{1}$$

where p_o is the saturation vapor pressure of the adsorbate, γ is its surface tension, and $\overline{V}$ is the molar volume of the adsorbate. If the vapor pressure of adsorbate over a porous adsorbent is increased to a value given by Eq. 1, the closed-end pores having radii equal to or smaller than r_k will be completely filled by capillary condensation. For the reverse process (i.e., if the vapor pressure is decreased to a given p/p_o value), completely filled pores having radii equal to or larger than r_k of Eq. 1 will empty. The equivalent pore radius r_p is calculated by Eq. 2 where r_k is an equivalent pore radius and t is the thickness of the film adsorbed on the surfaces of capillaries at any given p/p_o.

$$r_p = r_k + t \tag{2}$$

During an adsorption or desorption isotherm experiment, if the relative pressure is changed from $(p/p_o)_1$ to $(p/p_o)_2$, pores with corresponding Kelvin radii between r_{k1} and r_{k2} (Eq. 1) will either fill or empty depending on the sorption branch being adsorbed or desorbed respectively. That is accompanied by a change ΔV in the total volume of adsorbate V adsorbed by the porous adsorbent. Part of the change ΔV is due to adsorption or desportion of the adsorbate from the free surface as expressed below:

$$\Delta V = \Delta V_k + \Delta V_f \tag{3}$$

where ΔV_k is the volume adsorbed or desorbed because of capillary condensation (inner capillary or core volume) and ΔV_f is the volume of the adsorbate that is adsorbed or desorbed from the free surfaces and that results in a change of the thickness of the adsorbed film from t_1 to t_2 on free surfaces. The thickness t can be expressed in terms of the number of molecular layers n as follows:

$$t = n \cdot \delta \tag{4}$$

where δ is the thickness of one adsorbate molecule.

The volume ΔV_k is the volume of capillaries having radii from r_{k1} to r_{k2} exclusive of assumed adsorbed film in those capillaries, which is referred to as inner-capillary volume (11) or pore volume (16). Then, the net volume of capillaries ΔV_p, filled or emptied in this range, is expressed as

$$\Delta V_p = R_r \Delta V_k \tag{5}$$

where

$$R_r = (r_p/r_k)^2 \tag{6}$$

The adsorbate volume ΔV_f, desorbed from or adsorbed on the free surface for each p/p_o increment, is expressed as follows:

$$\Delta V_f = \Delta n \cdot \delta \cdot \Sigma A_p \tag{7}$$

where Δn is the number of the monomolecular layers adsorbed or desorbed from free surface, δ is the thickness of one molecule of the adsorbate, and A_p is the area of the empty pores or free surface. The latter is expressed as follows:

$$A_p = 2\Delta V_p/\bar{r}_p \tag{8}$$

where $\bar{r}_p$ is the average pore radius for the average relative vapor pressure $(\bar{p}/\bar{p}_o)$, as expressed in Eqs. 9 and 10.

$$\bar{r}_p = \frac{r_{p1} + r_{p2}}{2} \tag{9}$$

$$(\bar{p}/\bar{p}_o) = \frac{(p/p_o)_1 + (p/p_o)_2}{2} \tag{10}$$

After those relationships are established, the Pierce method proceeds with a set of calculations from sorption isotherms starting with $p/p_o = 1$ and t-curves leading to pore-size distribution, which is summarized in the steps below as it is used in the present paper with minor modifications.

1. p/p_o versus V is obtained from sorption isotherms.
2. n and t values are obtained from established t-curves for each p/p_o on the basis of BET parameter C, which is obtained from the BET plot of the sorption isotherm.
3. r_k values corresponding to each p/p_o are calculated from Eq. 1.
4. r_p values corresponding to each p/p_o are calculated from Eq. 2 and step 2.
5. R_r values are calculated from Eq. 6.
6. $\bar{r}_p$ values are calculated from Eq. 9 and step 4, the corresponding $(\bar{p}/\bar{p}_o)$ values are calculated from Eq. 10, and then $1/\bar{r}_p$ is plotted versus log $\bar{p}/\bar{p}_o$.
7. Δn values for each p/p_o increment are calculated from step 2.
8. ΔV values for each p/p_o increment are calculated from step 1.

a. ΔV_k value for the first sorption increment to $p/p_o = 1$ (if the adsorption branch is used) or from $p/p_o = 1$ (if the desorption branch is used) is determined from step 1. Because there is no free surface on a porous adsorbent at $p/p_o = 1$, i.e., all the pores are filled up by capillary condensation, $\Delta V_k = \Delta V$ and $\Delta V_f = 0$.

b. ΔV_p value for the first sorption increment is calculated from Eq. 5 and steps 5 and 8a.

c. $\bar{r}_p$ value for the first sorption increment is determined from the plot of step 6 by extrapolation.

d. A_p value for the first sorption increment is calculated from Eq. 8 and steps 8b and 8c. That value of A_p is to be used for the next sorption increment.

Results obtained in steps 6 and 8b constitute the coordinates of the first point of the pore-size distribution curve. The subsequent points are determined by the use of steps 1 to 8 and steps 9 to 14 given below:

9. ΔV_f values are calculated from Eq. 7 and steps 7 and 8d for the second sorption increment and from Eq. 7 and steps 7 and 14 for the subsequent sorption increments.
10. ΔV_k values are calculated from Eq. 3 and steps 8 and 9.
11. ΔV_p values are calculated from Eq. 5 and steps 5 and 10.
12. A_p values are calculated from Eq. 8 and steps 11 and 6.
13. $\Sigma\Delta V_p$ values are calculated from the results of step 11 (the summation is carried out from lowest p/p_o to $p/p_o = 1$).
14. ΣA_p values are calculated from the results of step 12.

Results obtained in steps 6 and 11 constitute the coordinates of pore-size distribution curves.

The original Pierce method (11) was developed for desorption isotherms of nitrogen. The t-curve data for nitrogen available to Pierce at that time were too high as reported by him later (22). The ambiguity of t-curve data that we believed existed all along has recently been eliminated by Brunauer and his coworkers (18, 21) enabling researchers to use not only nitrogen but other adsorbates. In the present work, water vapor was used as the adsorbate on the basis of the data of Brunauer et al. (21). Choice of water was made for 2 reasons: First, not all pores and surfaces of soil minerals are accessible to nitrogen, whereas they are to water vapor (21, 23, 24, 25); and, second, use of water vapor as adsorbate simplifies the experimental procedure. Other minor revisions of the Pierce method made in the present paper are use of both adsorption and desorption data for reasons to be explained later and determination of $\bar{r}_p$ for the first sorption increment from $p/p_o = 1$ as explained above in step 8c. Pierce (11) offers no explanation of how $\bar{r}_p$ for the first increment is obtained.

EXPERIMENTAL ANALYSIS

Instrumentation

The sorption isotherms were determined gravimetrically by the use of a Cahn RG electrobalance coupled with an automatic Sargent recorder. The sample weight was determined to microgram sensitivity. The instrument was calibrated prior to the test, and a buoyancy correction was applied. Room temperature was maintained at 22 ± 0.25 C throughout the investigation.

A capacitance manometer was used to prevent mercury contamination and to maintain a pure adsorbent-adsorbate system. It operated as a null indicator for the system. The true pressure was read from a mercury manometer with a vernier micrometer slide cathotometer. The pressures are accurate to 1 μm of mercury.

A rotary mechanical fore pump and an oil diffusion pump provided a vacuum of 10^{-6} torr. The sample was suspended from an arm of the microbalance into a glass hang-down tube immersed in a constant temperature bath maintained at 20.00 ± 0.01 C. Temperature readings were taken with a Beckman thermometer, accurate to ± 0.002 C. The Beckman thermometer was calibrated against a thermometer, certified by the National Bureau of Standards, at the thermostat temperature. The detailed description of the system is given elsewhere (26, 27).

Experimental Procedure

The sample in the system was evacuated for 2 weeks at a room temperature of 22 C. The hang-down tube containing the sample and all parts of the adsorption system except the microbalance were heated for 12 hours to about 300 C. The sample was heated occasionally during degassing with an infrared heater. The water in the reservoir was also degassed during the period of evacuation after it was frozen in liquid nitrogen; that was done at least 5 times until no dissolved air was left. When the system reached 10^{-6} torr (determined with a calibrated discharge gauge), the pumping valve was closed for 2 hours to determine whether degassing was complete. The part of the system con-

nected to the capacitance manometer was also pumped down at the same time. Finally, the system was sealed, and the capacitance manometer was calibrated.

Water vapor was transferred into the system from the water reservoir in the range of $p/p_o = 0$ to $p/p_o = 1$. The amount of water adsorbed on the sample was automatically registered on the recorder, and the water vapor pressure was determined. System equilibrium was attained when there was no increase in sample weight and no drop of system pressure. A 24-hour period was allowed to ensure that equilibrium had occurred.

The desorption isotherms were obtained by condensing more and more vapor back into the water reservoir. That condensation process was performed by cooling the water reservoir first with an ice-water mixture and then with a dewar flask containing liquid nitrogen.

Materials Used

The soil sample used in the present study was an undisturbed hand-carved friable Iowa loess obtained from Prospect Hill in Sioux City, Iowa. Its engineering properties are given in Table 1. Its dry density and porosity were determined from bulk dimensions and oven-dry weight of hand-carved specimens.

RESULTS AND DATA ANALYSIS

The water sorption isotherms of the undisturbed loess sample at 20 C exhibit a strong hysteresis (Fig. 1). BET plots of sorption data are shown in Figure 2. The BET parameters V_m and C calculated from Figure 2 are 0.0135 cm^3/g and 20 for the adsorption branch and 0.0180 cm^3/g and 54.7 for the desorption branch respectively. The total specific surface of the sample calculated from the BET parameter V_m is 48.7 m^2/g from the adsorption isotherm and 64.8 m^2/g from the desorption isotherm. The specific surface calculated from the desorption isotherm is about 33 percent higher than that calculated from the adsorption isotherm.

Pore-size distribution data are given in Tables 2 and 3 for adsorption and desorption respectively. Data are compiled in those tables in accordance with the 14-step procedure described earlier. The statistical number of layers n are obtained from Hagymassy, Brunauer, and Mikhail (21). A plot of $\log \bar{p}/\bar{p}_o$ versus $1/\bar{r}_p$ is shown in Figure 3, which was used to obtain $\bar{r}_p$ value for the first sorption increments from $p/p_o = 1$.

Hysteresis Loop

The identification of the true equilibrium branch of sorption isotherms of porous solids has been a subject of argument for more than half a century (24, 17). Those rejecting the adsorption branch base their arguments on either Zsigmondy's explanation of incomplete wetting during adsorption due to impurities or on Foster's explanation of delayed nucleation of menisci in open-ended capillaries in the range of capillary condensation during the adsorption process. Those rejecting the desorption branch base their arguments on McBain's explanation of delayed desorption of the adsorbate trapped in pores with narrow necks shaped like ink bottles. Although each constitutes a partial explanation, together they constitute a reasonable explanation of sorption hysteresis in general. The Zsigmondy explanation gives rise to a diagnostic irreversible hysteresis and can be eliminated by drastic evacuation, whereas the Foster and McBain explanations cause permanent reversible hysteresis. The latter two types, however, if coexisting, defy the existence of an equilibrium branch.

In making a choice, therefore, one must examine the system by assessing to what extent each of those types may be effective and if one of them may be considered negligible. Such an examination has been presented by Brunauer et al. (17). It led them to use the adsorption branch for pore-structure analysis of hardened portland cement pastes; however, the desorption branch has found large-scale acceptance in the literature. In the present work the adsorption isotherm has been used as the branch closest to equilibrium. Zsigmondy hysteresis is believed to be minimized by the drastic evacuation. The choice, then, between Foster and McBain was made on the basis of the

Figure 1. Sorption isotherms of water vapor on friable loess.

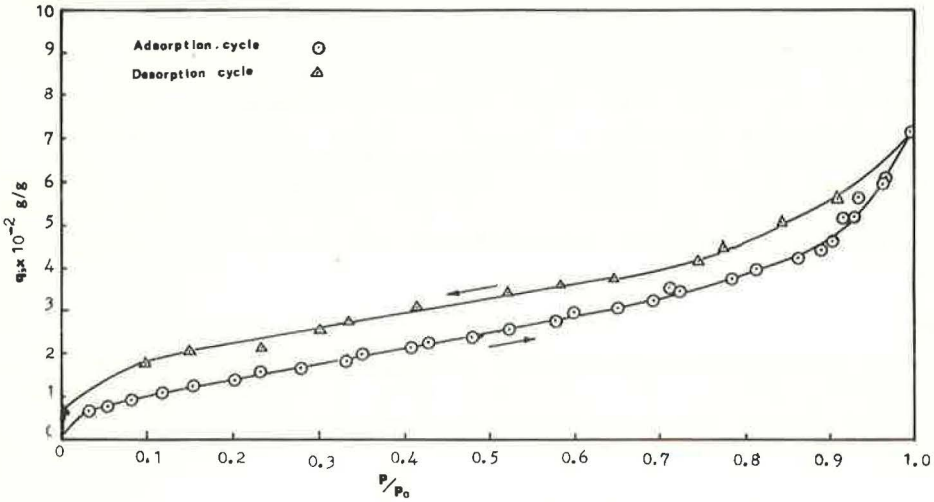

Table 1. Properties of friable Iowa loess.

Property	Amount
Specific gravity	2.7[a]
Undisturbed dry density, lb/ft^3	85.3
Undisturbed porosity, percent	49.4
Undisturbed void ratio, cm^3/cm^3	0.975
Undisturbed void volume, cm^3/g	0.361
Liquid limit, percent	30
Plastic limit, percent	26
Standard Proctor compaction	
Optimum moisture, percent	16.5
Maximum dry density, lb/ft^3	109.4
Grain-size distribution, percent	
Clay (< 2 μm)	14
Silt (2 to 74 μm)	86
AASHO classification	A-4(8)
Field moisture, percent	7 to 10
Strength parameters	
Internal friction angle, deg	32.2
Cohesion, lb/in.^{2}	1.0
Minerals present (X-ray analysis)	Quartz, montmorillonite illite, calcium carbonate, dolomite, and feldspar

[a]Average of 9 tests.

Figure 2. BET for water vapor on friable loess.

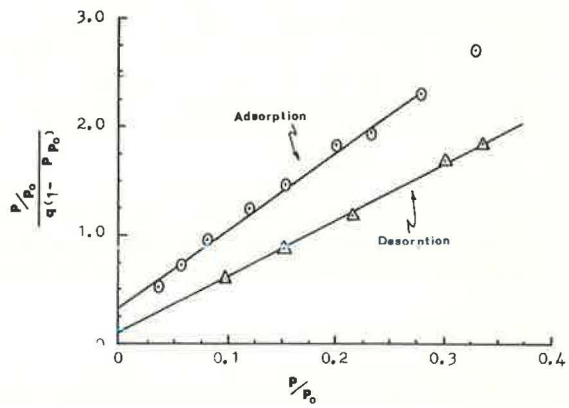

Table 2. Pore-size distribution analysis of undisturbed loess sample—adsorption.

Step	Parameter	Values for Each Increment														
1	p/p_o	1.000	0.963	0.926	0.901	0.862	0.812	0.682	0.597	0.479	0.407	0.333	0.234	0.155	0.083	0
	V, cm^3/g	0.0713	0.0607	0.0518	0.0464	0.0426	0.0395	0.0327	0.0297	0.0240	0.0213	0.0184	0.0157	0.0127	0.0094	0
2	n	6.05	4.45	3.85	3.56	3.17	2.80	2.30	1.98	1.75	1.57	1.41	1.17	0.95	0.72	0
	t, Å	18.15	13.35	11.55	10.68	9.51	8.40	6.90	5.94	5.25	4.71	4.23	3.51	2.85	2.16	0
3	r_k, Å		0.270	140	1.05	73	51	28	20	12.5	11.0	9.5	7.5	5.8	4	0
4	r_p, Å		283.35	151.55	115.68	82.51	59.40	34.90	25.94	17.75	15.71	13.73	11.01	8.65	6.16	
5	$\frac{R_r}{}$		1.10	1.17	1.21	1.28	1.35	1.55	1.67	2.01	2.04	2.08	2.14	2.25	2.36	
6	$\frac{p/p_o}{\bar{r}_p}$, Å	0.979 (625)[a]	0.944 217.45	0.913 133.61	0.881 99.09	0.837 70.95	0.752 47.65	0.644 30.42	0.538 21.84	0.443 16.73	0.370 14.97	0.283 12.37	0.194 9.83	0.119 7.40	0.041 3.08	
7	Δn	1.41	0.60	0.29	0.39	0.37	0.50	0.32	0.23	0.18	0.16	0.24	0.22	0.23	0.72	
8	ΔV, cm^3/g	0.0106	0.0089	0.0054	0.0038	0.0031	0.0068	0.0030	0.0057	0.0027	0.0029	0.0027	0.0030	0.0033	0.0094	
9	ΔV_t, cm^3/g	0	0.0001	0.0001	0.0002	0.0003	0.0006	0.0008	0.0007	0.0010	0.0011	0.0020	0.0020	0.0024	0.0089	
10	ΔV_k, cm^3/g	0.0106	0.0088	0.0053	0.0035	0.0027	0.0061	0.0022	0.0050	0.0016	0.0018	0.0007	0.0010	0.0009	0.0005	
11	ΔV_p, cm^3/g	0.0116	0.0103	0.0064	0.0045	0.0037	0.0095	0.0036	0.0100	0.0033	0.0037	0.0015	0.0022	0.0021	0.0020[b]	
12	A_p, m^2/g	0.37	0.95	0.96	0.91	1.05	4.00	2.41	9.20	3.97	5.00	2.42	4.58	5.68	7.16[b]	
13	$\Sigma\Delta V_p$, cm^3/g	0.0744	0.0628	0.0525	0.0461	0.0416	0.0379	0.0284	0.0246	0.0148	0.0115	0.0078	0.0063	0.0041	0.0020	
14	ΣA_p, m^2/g	0.37	1.32	2.28	3.19	4.24	8.24	10.65	19.85	23.82	28.82	31.24	35.82	41.51	48.67[b]	

[a]Obtained from Figure 3.

[b]Based on the total BET specific surface area of 48.67 m^2/g as follows: $A_p = 48.67 - 41.51 = 7.16$ m^2/g; and $\Delta V_p = \Delta V_k + \Delta n \times \delta \times A_p = 0.005 + 0.72 \times 3 \times 10^{-4} \times 7.16 = 0.0020$ cm^3/g.

following argument: In consolidated fine-particulate systems, such as clayey soils, particle-to-particle contacts are believed to be intimate enough to furnish the seat for meniscus nucleation through multilayer adsorption in the early stages of adsorption, eliminating most of the open-ended pores and producing an ink-bottle type of pore. Persistence of the hysteresis to the origin supports that assumption.

Pore-Surface and Pore-Volume Distributions

The values of A_p calculated from adsorption and desorption isotherms are shown in Figure 4. Data shown in Figure 4 and given in Tables 2 and 3 reveal that (a) about 80 percent of the total surface area is located in capillaries smaller than 28 Å in radius; and (b) the largest concentration of the surface area is found in small capillaries of 10 and 50 Å in diameter.

Pore-volume distribution curves corresponding to adsorption and desorption isotherms are shown in Figures 5 and 6. Based on the assumption that the adsorption isotherm is the equilibrium branch, curve A shown in Figure 5 or Figure 6 represents the correct pore-size distribution and curve D represents the size distribution of bottle necks on an exaggerated scale, i.e., as if the voids constricted by the bottle necks are all of neck diameter. Thus, the difference between the 2 curves can be taken as an indication of the extent of constrictions in the pore structure.

The pore-size distribution obtained from the adsorption isotherm is combined with the pore-size distribution of the same friable loess sample obtained by mercury injection (13, 14) shown in Figures 7 and 8. The agreement between the lower end of the distribution function curve obtained from the adsorption isotherm (Fig. 7) is quite striking. Also, the smooth transition between the cumulative percentage of pore-volume distribution curves obtained by the 2 methods (Fig. 8) shows that mercury injection and adsorption isotherm methods are compatible. Percentage of cumulative pore volumes was calculated as percentages of the total pore volume 0.361 cm^3/g (Table 1).

DISCUSSION OF RESULTS

The gross results of pore-size distribution analysis are given in Table 4. The combined average pore-diameter range (covered by both the sorption isotherm and the mercury-injection methods) extends from about 6×10^{-4} to 32 μm accounting for about 91 percent of the total void volume determined from bulk properties of the sample (Table 1). The adsorption isotherm method accounts for about 20 percent and mercury injection for about 73 percent of that volume with an overlap in the range of 0.0585 to 0.0625 μm radius covering about 2 percent of the total voids (Fig. 8). The upper limit of average pore radius of 16 μm (32 μm in diameter) corresponds to the volume injected by mercury in the pressure range of 5 to 10 lb/in^2. Because the mercury-injection data in the range of 0 to 1 lb/in^2 were open to question and because the average pore radius in that range is indeterminate, the data corresponding to that range have been excluded from the present paper. The volume of the pores having diameters larger than 32 μm was then found to be about 9 percent after the curves of the 2 methods were superimposed as shown in Figure 8.

Comparison of the specific surface areas obtained from pore-size analysis with those obtained from BET plots has been a generally accepted criterion for assessment of the dependability of the pore analysis. Another criterion is the comparison of the total volume determined from pore analysis with that directly determined from sorption isotherms. Those criteria have been criticized by Brunauer (18). The pore-size analysis can only be as accurate as the BET analysis and as the total volume of adsorbate determined at $p/p_o = 1$. Any large deviation beyond those due to the pore-shape considerations and experimental error should be attributable to the assumed boundaries, i.e., the upper and the lower ends of the p/p_o range covering the capillary condensation. For example, if the lower boundary of p/p_o was taken as 0.333 (Table 2), the total surface area ΣA_p would have a value of 28.82 m^2/g and the total pore volume $\Sigma \Delta V_p$ would be 0.0103 cm^3/g as compared to the BET area of 48.67 m^2/g and the total pore volume of 0.0713 cm^3/g.

Table 3. Pore-size distribution analysis of undisturbed loess sample—desorption.

Step	Parameter	Values for Each Increment														
1	p/p_o	1.0	0.909	0.842	0.772	0.745	0.661	0.582	0.518	0.411	0.336	0.304	0.216	0.153	0.097	0
	V, cm^3/g	0.0713	0.0555	0.0508	0.0449	0.0413	0.0387	0.0376	0.0360	0.0341	0.0306	0.0277	0.0232	0.0205	0.0179	0.0063
2	n	6.06	3.65	3.05	2.60	2.48	2.20	2.15	1.96	1.72	1.60	1.45	1.26	1.17	1.03	
	t, Å	18.18	10.95	9.15	7.80	7.44	6.60	6.45	5.88	5.16	4.80	4.35	3.78	3.51	2.09	
3	r_k, Å		115	62	40	35	25	23	19	15	11.5	10.0	7.3	6.0	4.8	0
4	r_p, Å		125.95	71.15	47.80	42.44	31.60	29.45	24.88	20.16	16.30	14.35	11.08	9.51	7.89	
5	R_r	1.00	1.20	1.31	1.42	1.47	1.59	1.64	1.72	1.80	2.00	2.06	2.30	2.51	2.70	
6	$\overline{p/p_o}$	0.954	0.875	0.807	0.758	0.703	0.621	0.550	0.464	0.373	0.320	0.260	0.184	0.125	0.048	
	$\overline{r}_p$, Å	(312)[a]	98.55	59.47	45.12	37.02	30.52	22.52	18.23	15.32	13.77	12.14	10.29	8.70	3.95	
7	Δn	2.41	0.60	0.35	0.12	0.28	0.05	0.24	0.24	0.12	0.15	0.19	0.09	0.14	1.03	
8	ΔV, cm^3/g	0.0158	0.0047	0.0059	0.0036	0.0026	0.0011	0.0016	0.0019	0.0035	0.0029	0.0045	0.0027	0.0026	0.0116	
9	ΔV_r, cm^3/g	0	0.0002	0.0003	0.0002	0.0006	0.0001	0.0007	0.0008	0.0005	0.0009	0.0015	0.0010	0.0020	0.0104	
10	ΔV_k, cm^3/g	0.0158	0.0045	0.0056	0.0034	0.0020	0.0010	0.0009	0.0011	0.0030	0.0020	0.0030	0.0017	0.0006	0.0012	
11	ΔV_p, cm^3/g	0.0189	0.0059	0.0079	0.0050	0.0032	0.0016	0.0016	0.0020	0.0060	0.0041	0.0069	0.0043	0.0016	0.0054[b]	
12	A_p, m^2/g	1.21	1.20	2.70	2.23	1.72	1.07	1.37	2.19	7.83	5.96	11.38	6.54	3.68	13.72	
13	$\Sigma\Delta V_p$, cm^3/g	0.0744	0.0555	0.0496	0.0417	0.0367	0.0335	0.0319	0.0303	0.0283	0.0223	0.0182	0.0113	0.0070	0.0054	
14	ΣA_p, m^2/g	1.21	2.41	5.11	7.34	9.06	10.13	11.50	13.69	21.52	27.48	38.86	47.40	51.08	64.80[b]	

[a] Obtained from Figure 3.
[b] Based on the total BET specific surface area of 64.80 as follows: $A_p = 64.80 - 51.08 = 13.72\ m^2/g$; and $\Delta V_p = \Delta V_k + \Delta n \times \delta \times A_p = 0.0012 + 1.03 \times 3 \times 10^{-4} \times 13.72 = 0.0054\ cm^3/g$.

Figure 3. p/p_o versus $1/\overline{r}_p$.

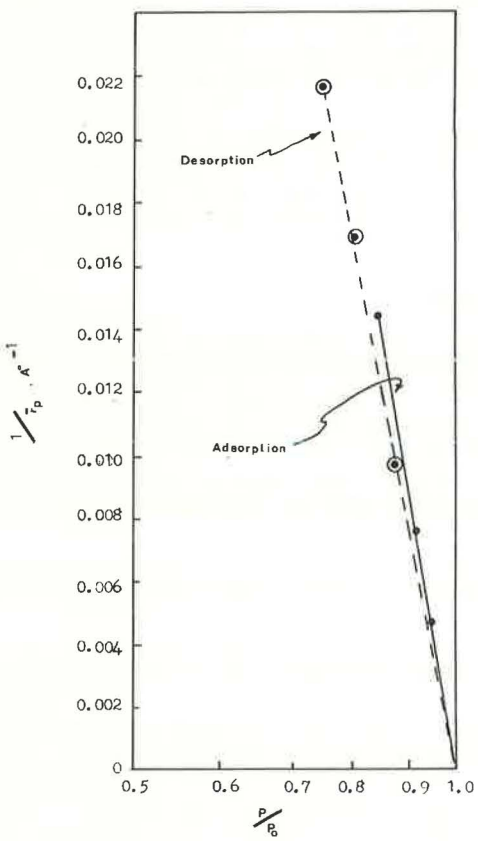

Figure 4. Surface-area distribution of friable loess.

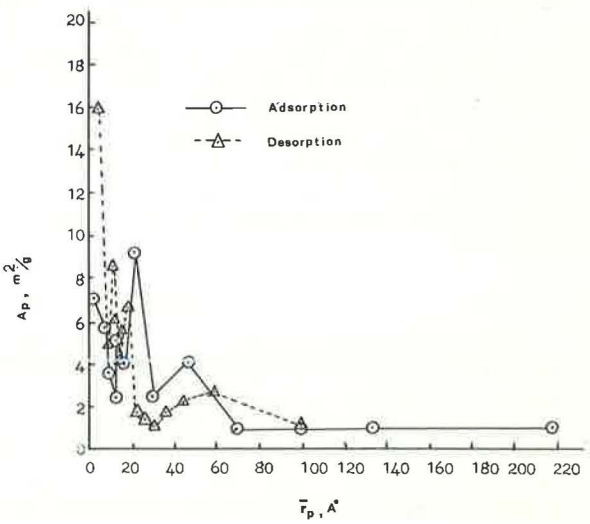

Figure 5. Pore-volume distribution of friable loess.

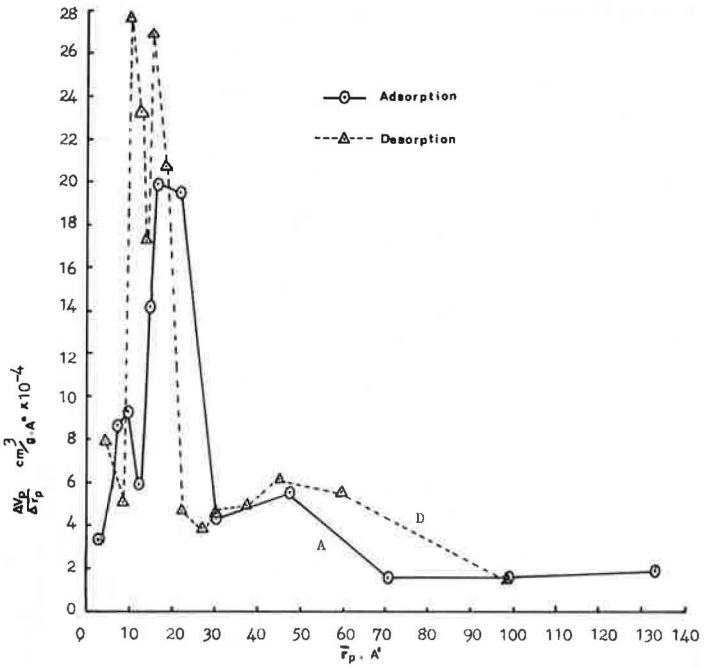

Figure 6. Cumulative pore-volume distribution of friable loess.

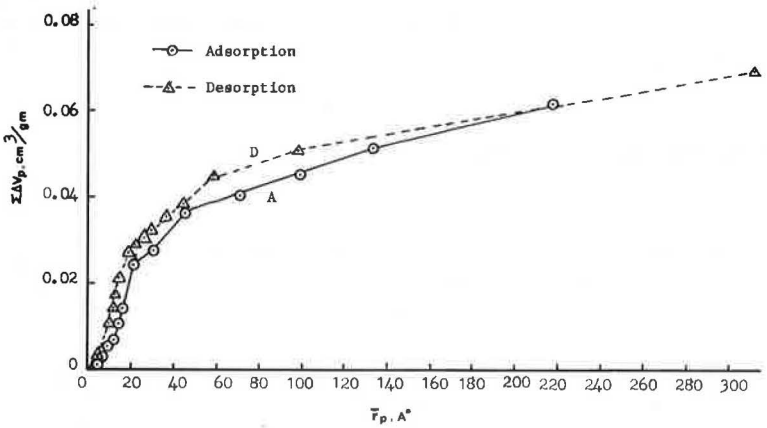

Table 4. Summary of pore-size analysis of friable Iowa loess.

Method	$\Sigma\Delta V_p$ (cm^3/g)	Specific Surface Area (m^2/g)	Average Pore Radius (μm) Lower Limit	Upper Limit	$\frac{\Sigma\Delta V_p}{V_t}$
Sorption isotherm pore analysis					
Adsorption	0.0744	48.7*	3.1×10^{-4}	0.063	0.203
Desorption	0.0744	64.8*	4.0×10^{-4}	0.0312	0.203
Mercury injection pore analysis	0.265		0.058	16.0	0.734
Sorption isotherm and BET analysis					
Adsorption	0.0713	48.7			0.198
Desorption	0.0713	64.8			0.198
Bulk properties	0.361				1.00

Note: $\Sigma\Delta V_p$ is the total pore volume, and V_t is the total pore volume determined from bulk properties.

*Assumed to be equal to BET specific surface area as a necessary condition.

Figure 7. Combined pore-volume distribution of friable loess.

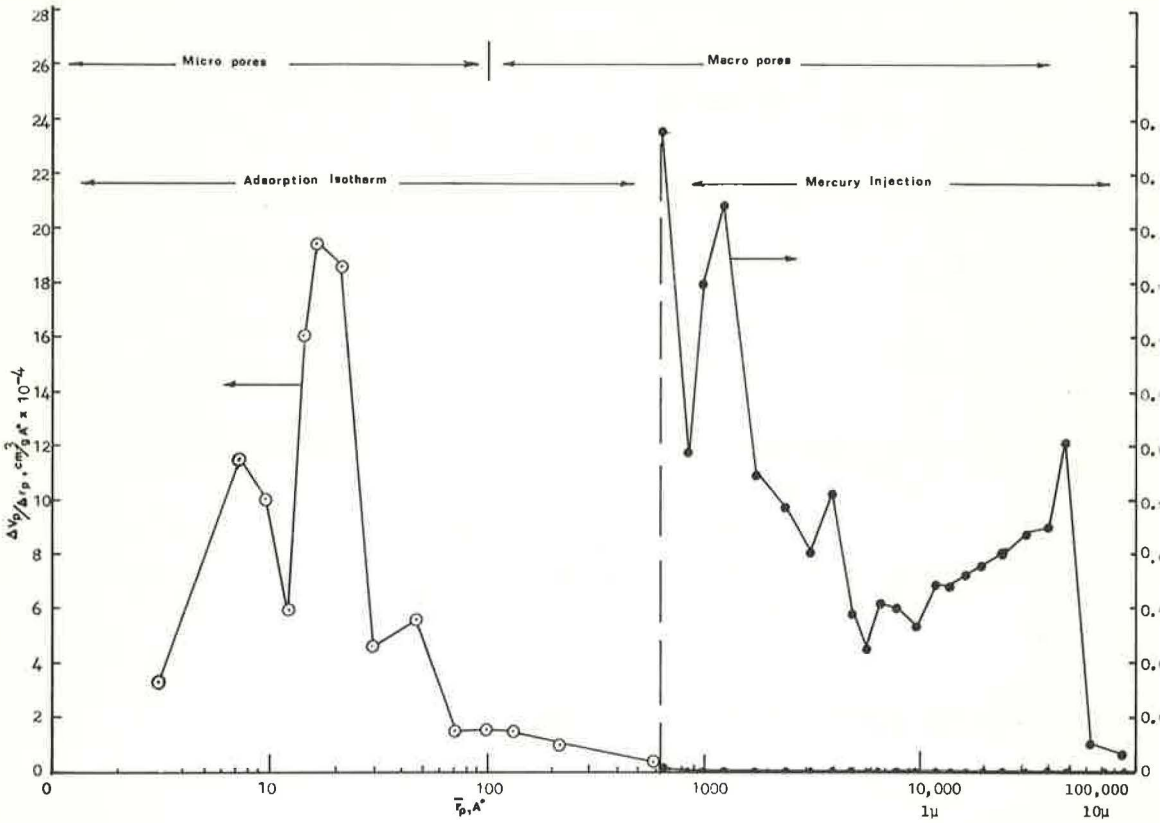

Figure 8. Normalized cumulative pore-volume curve of friable loess.

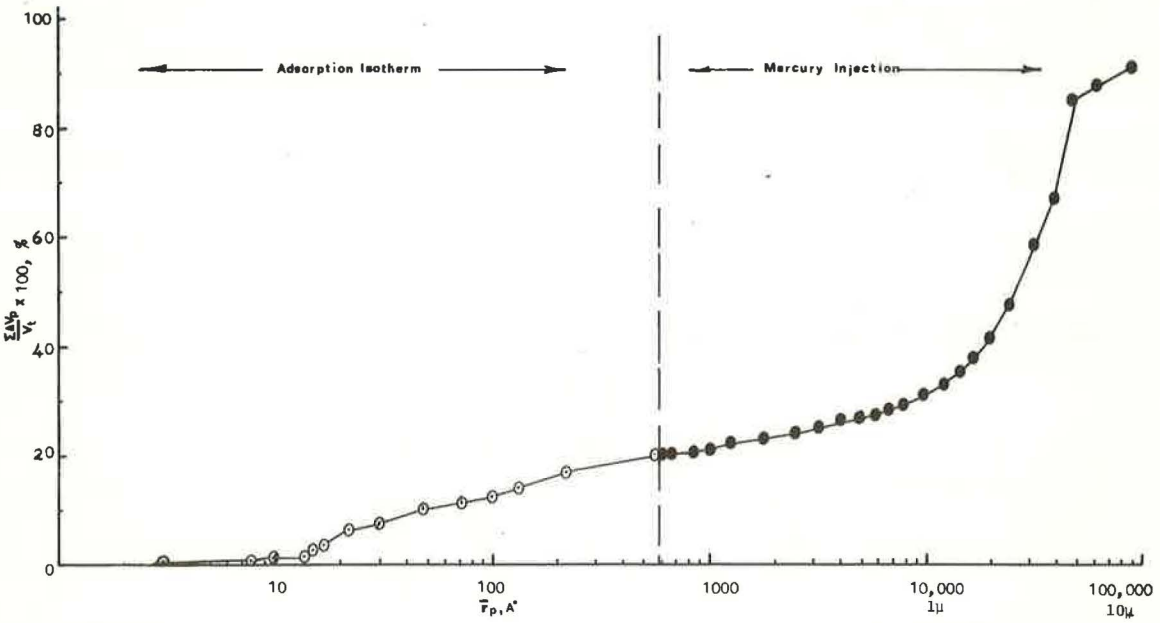

Normally pore-size analysis is carried to the point where the hysteresis loop is closed on the assumption that the hysteresis loop covers the range of all pore sizes. But an agreement between the results of pore analysis and BET specific surface area, i.e., total pore volume, is not always obtained, and seldom are significant differences between the 2 results observed. According to Brunauer et al. (18), that difference can be attributed to micropores smaller than 15 Å in diameter, which fill by multilayer adsorption. In the present paper, total specific surface and total pore volume agreements are used as a necessary condition to be fulfilled, and the last p/p_o increment was chosen so that this criterion is met. To do that, the calculation procedure for the last p/p_o increment (last column of Table 2 or Table 3) was modified and the incremental area A_p was calculated as a difference between BET specific surface and total pore area calculated to the last increment, $A_{BET} - \Sigma A_p$.

From the sorption isotherm, the total volume of pores filled at saturation relative pressure ($p/p_o = 1$) is 0.0713 cm^3/g, which is about 20 percent of the total pore volume of 0.361 cm^3/g determined from bulk properties. Evidently very large pores do not fill by capillary condensation, either because of slow condensation rates or more likely because large open-ended pores with plane surfaces inhibit nucleation of menisci.

The loess used contained 14 percent of clay sizes in which unknown amounts of expansive montmorillonite were present (Table 1). The expansive characteristics of expanding 3-layer clays such as montmorillonite may be a damaging factor in pore-size distribution analysis in which water vapor is used as an adsorbate. However, from the pore-size distribution curves and the cumulative pore-volume curve of friable loess used, the authors found no evidence of expansion. It is suggested that use of water vapor and void-expanding-inert vapors, i.e., nitrogen, as adsorbate may be extremely essential in distinguishing the expansive extension of the soils under investigation. Further research is needed in applying the modified Pierce's method in conjunction with mercury-injection porosimetry to various nonexpansive and expansive soils.

SUMMARY AND CONCLUSIONS

A method using sorption isotherm data to analyze pore-size distribution is presented. The method, combined with a mercury porosimetry technique, indicates that pore-size distribution can be determined. The main findings of this investigation are summarized below.

1. The Pierce method was modified and advanced to determine pore-size distribution of a friable Iowa loess using water-sorption isotherm data. The method can be used for different adsorbates on different soil materials.
2. Both adsorption and desorption branches were used for pore-size distribution analysis. The difference between the 2 branches was interpreted as an indication of the extent of constrictions within the pore structure according to McBain's ink-bottle theory.
3. Pore-size distribution curves obtained from the adsorption isotherm were compatible with mercury porosimetry results. Practically, the adsorption isotherm method covers the pores from 0 to 600 Å in radius, and the mercury-injection method covers the rest of the bigger pores.
4. The pore-size distribution of soil may be significant in the analysis of soil structure in relation to permeability, cohesion, and surface activity of the soil matter.

ACKNOWLEDGMENTS

The authors gratefully acknowledge the support given by the Environmental Sciences Division, Army Research Office, Durham, North Carolina. The authors would also like to acknowledge the sponsorship of the Engineering Research Institute at Iowa State University. The senior author acknowledges NASA for the partial financial support from the National Aeronautics and Space Administration.

REFERENCES

1. Mitchell, J. K. The Fabric of Natural Clays and Its Relation to Engineering Properties. HRB Proc., Vol. 35, 1956, pp. 693-713.
2. Skempton, A. W. Long-Term Stability of Clay Slopes. Geotechnique, Vol. 14, 1964, pp. 75-102.
3. Diamond, S. Pore-Size Distribution in Clays. Clays and Clay Miner., Vol. 13, No. 1, 1970, pp. 7-23.
4. Sridharan, A., Altschaeffl, A. G., and Diamond, S. Pore Size Distribution Studies. J. Soil Mech. and Found. Div., Proc. ASCE., Vol. 97 No. SM5, 1971, pp. 771-787.
5. Washburn, E. W. Note on a Method of Determining the Distribution of Pore Sizes in a Porous Material. Nat. Acad. Sci. Proc, Vol. 7, 1921, pp. 115-116.
6. Ritter, H. L., and Drake, L. C. Pore-Size Distribution in Porous Materials; Pressure Porosimeter and Determinations of Complete Macropore-Size Distribution. Ind. Eng. Chem. Anal. Ed., Vol. 17, 1945, pp. 782-786.
7. Wheeler, A. Reaction Rates and Selectivity in Catalyst Pores. Adv. in Catalysis and Relat. Subj., Vol. 3, 1951, pp. 249-327.
8. Wheeler, A. Reaction Rates and Selectivity in Catalyst Pores. Catalysis, Vol. 2, 1955, pp. 105-123.
9. Oulton, T. D. The Pore Size-Surface Area Distribution of a Cracking Catalyst. J. Phys. Chem., Vol. 52, 1948, pp. 1296-1314.
10. Barrett, E. P., Joyner, L. G., and Halenda, P. P. The Determination of Pore Volume and Area Distribution in Porous Substances: I—Computations From Nitrogen Isotherms. J. Am. Chem. Soc., Vol. 73, 1951, pp. 373-380.
11. Pierce, C. Computation of Pore Sizes From Physical Adsorption Data. J. Phys. Chem., Vol. 57, 1953, pp. 149-152.
12. Cranston, R. W., and Inkley, F. A. The Determination of Pore Structures From Nitrogen Adsorption Isotherms. Adv. in Catalysis and Relat. Subj., Vol. 9, 1957, pp. 143-154.
13. Badger, W. W. Structure of Friable Iowa Loess. Library, Iowa State Univ., Ames, PhD thesis, 1972.
14. Badger, W. W., and Lohnes, R. A. Structure of Friable Iowa Loess. Paper presented at HRB 52nd Annual Meeting and published in this Record.
15. Brunauer, S., Emmett, P. H., and Teller, E. Adsorption of Gases in Multimolecular Layers. J. Am. Chem. Soc., Vol. 60, 1938, pp. 309-319.
16. Brunauer, S., Mikhail, R. S., and Bodor, E. E. Pore Structure Analysis Without a Pore Shape Model. J. Colloid and Interf. Sci., Vol. 24, 1967, pp. 451-463.
17. Brunauer, S., Mikhail, R. S., and Bodor, E. E. Some Remarks About Capillary Condensation and Pore Structure Analysis. J. Colloid and Interf. Sci., Vol. 25, 1967, pp. 353-358.
18. Mikhail, R. S., Brunauer, S., and Bodor, E. E. Investigation of a Complete Pore-Structure Analysis: I—Analysis of Micropores. J. Colloid and Interf. Sci., Vol. 26, 1968, pp. 45-53.
19. Mikhail, R. S., Brunauer, S., and Bodor, E. E. Investigations of a Complete Pore-Structure Analysis: II—Analysis of Four Silica Gels. J. Colloid and Interf. Sci., Vol. 26, 1968, pp. 54-61.
20. Skalny, J., Bodor, E. E., and Brunauer, S. Investigations of a Complete Pore-Structure Analysis: III—Analysis of Carbon Adsorbents. J. Colloid and Interf. Sci., Vol. 37, No. 2, 1971, pp. 476-483.
21. Hagymassy, J., Jr., Brunauer, S., and Mikhail, R. S. Pore Structure Analysis by Water Vapor Adsorption. J. Colloid and Interf. Sci., Vol. 29, No. 3, 1969, pp. 485-491.
22. Pierce, C. Effect of Interparticle Condensation on Heats of Adsorption and Isotherms of Powder Samples. J. Phys. Chem., Vol. 63, 1959, pp. 1076-1079.
23. Emmett, P. H., Brunauer, S., and Love, K. S. The Measurement of Surface Area of Soils and Soil Colloids by Use of Low Temperature van der Waal's Adsorption Isotherms. Soil Sci., Vol. 45, 1938, pp. 57-65.

24. Brunauer, S. The Adsorption of Gasses and Vapors. In Physical Adsorption, Princeton Univ. Press, 1943.
25. Demirel, T. Adsorption of Water Vapor by Sodium and Calcium Montmorillonites. Iowa State Univ., Ames, PhD theses, 1962.
26. Senich, D., Demirel, T., and Handy, R. L. X-Ray Diffraction and Adsorption Isotherm Studies of the Calcium Montmorillonite-H_2O System. Highway Research Record 209, 1967, pp. 23-54.
27. Huang, R. J., Demirel, T., and McGee, T. D. The Adsorption of Water Vapor on E-Glass. J. Am. Ceram. Soc., Vol. 55, No. 8, 1972, pp. 399-405.